Computational and Structural Biotechnology Journal 21 (2023) 3827–3840

Contents lists available at ScienceDirect

Computational and Structural Biotechnology Journal

journal homepage: www.elsevier.com/locate/csbj

Research article

Machine learning-based identification of lower grade glioma stemness subtypes discriminates patient prognosis and drug response

Hongshu Zhou [a,b], Bo Chen [a,b,c], Liyang Zhang [a,b,d,e], Chuntao Li [a,b,d,e,*]

[a] Department of Neurosurgery, Xiangya Hospital, Central South University, Changsha, Hunan, PR China
[b] Hypothalamic-pituitary Research Center, Xiangya Hospital, Central South University, Changsha, Hunan, PR China
[c] Department of Surgery, School of Clinical Medicine, LKS Faculty of Medicine, The University of Hong Kong, Queen Mary Hospital, Hong Kong SAR, China
[d] Clinical Diagnosis and Therapy Center for Glioma, Xiangya Hospital, Central South University, Changsha, Hunan, PR China
[e] National Clinical Research Center for Geriatric Disorders, Xiangya Hospital, Central South University, Changsha, Hunan, PR China

ARTICLE INFO

Keywords:
Lower grade glioma
Stemness
Subtype
Machine learning
Prognosis

ABSTRACT

Glioma stem cells (GSCs) remodel their tumor microenvironment to sustain a supportive niche. Identification and stratification of stemness related characteristics in patients with glioma might aid in the diagnosis and treatment of the disease. In this study, we calculated the mRNA stemness index in bulk and single-cell RNA-sequencing datasets using machine learning methods and investigated the correlation between stemness and clinicopathological characteristics. A glioma stemness-associated score (GSScore) was constructed using multivariate Cox regression analysis. We also generated a GSC cell line derived from a patient diagnosed with glioma and used glioma cell lines to validate the performance of the GSScore in predicting chemotherapeutic responses. Differentially expressed genes (DEGs) between GSCs with high and low GSScores were used to cluster lower-grade glioma (LGG) samples into three stemness subtypes. Differences in clinicopathological characteristics, including survival, copy number variations, mutations, tumor microenvironment, and immune and chemotherapeutic responses, among the three LGG stemness-associated subtypes were identified. Using machine learning methods, we further identified genes as subtype predictors and validated their performance using the CGGA datasets. In the current study, we identified a GSScore that correlated with LGG chemotherapeutic response. Through the score, we also identified a novel classification of the LGG subtype and associated subtype predictors, which might facilitate the development of precision therapy.

1. Introduction

Gliomas are the most common primary malignancy of the central nervous system. They are commonly derived from neuroglial stem or progenitor cells and have an incidence rate of 6.6 per 100,000 person [1]. The 2016 World Health Organization (WHO) glioma classification incorporated molecular biomarkers and histological features into an integrated diagnosis to better define glioma entities[2]. Lower-grade gliomas (LGGs) present highly variable clinical outcomes, with a median overall survival (OS) of 78.1 months[3,4]. Mutations in *IDH, TP53*, *ATRX* and 1p/19q codeletion are implicated in the prognosis of LGG. Current treatment methods include maximal surgical resection, concurrent chemoradiotherapy, adjuvant temozolomide (TMZ) therapy, and tumor treating fields, if available[5]. The identification of diagnostic and prognostic markers and risk factors is a trend in glioma research and may pave the way toward precision medicine[3,6,7].

Cancer stem cells (CSCs) possess self-renewal and differentiation abilities[8]. These cells are more likely to be preserved as small populations and generate differentiated progeny that constitute the tumor mass. Moreover, CSCs are more resistant to existing anticancer therapies, which is consistent with their role in relapse after therapy[9]. Glioma stem cells (GSCs) are a subpopulation of glioma cells with CSC characteristics, such as self-renewal, radio-chemoresistance, and drug resistance[10,11]. Functionally identified GSC markers include CD133, CD44, SSEA1, L1CAM, CD49f, A2B5, PDGFRA, and EGFR[11]. Recently, new therapeutic strategies targeting GSCs have been studied in depth, including tumor treating fields, antiangiogenesis therapy, and immunotherapy[4,12]. Inflammatory corpuscles, macrophages, and

* Correspondence to: Department of Neurosurgery, Hypothalamic-pituitary Research Center, Xiangya Hospital, Central South University, No. 87 Xiangya Rd, Changsha 410008, PR China.
E-mail address: chuntao.li@csu.edu.cn (C. Li).

https://doi.org/10.1016/j.csbj.2023.07.029
Received 6 March 2023; Received in revised form 6 July 2023; Accepted 19 July 2023
Available online 22 July 2023

cytokines, which comprise the tumor microenvironment (TME), play a crucial role in tumor initiation and progression[13]. GSCs typically reside in TME niches exposed to harsh conditions, such as hypoxia, acidic stress, and/or nutrient restriction. Conversely, GSCs engage in complex crosstalk with and aggressively remodel their TME to sustain a supportive niche[14]. The common presence of both hypoxic conditions and GSCs in perinecrotic cells suggests a correlation between the glioma microenvironment and cell stemness[15].

In this study, we intended to derive a new characterization of LGG stemness with better concentration on malignant cells, explore the relationship of LGG stemness with TME, and identify gene markers able to characterize stemness. Therefore, we used bulk and single-cell RNA-sequencing to evaluate the mRNA stemness index (mRNAsi)[8,16] of patients with LGG and its correlation with clinicopathological characteristics. We then calculated glioma stemness-associated scores (GSScores) using multivariate Cox regression analysis and divided The Cancer Genome Atlas (TCGA) LGG samples into three subtypes. The subtypes showed significantly different prognoses and immune cell infiltrations. We further used machine learning methods to identify genes important for stemness clustering (Supplementary Fig. S1). A patient-derived glioma stem cell (GSC) line and a glioma cell line were used to evaluate drug response, demonstrating that the GSScore is predictive of chemotherapeutic responses in glioma cell lines.

In conclusion, this work provides a GSScore that predicts chemotherapeutic response in glioma cell lines and identifies a novel classification of LGG subtypes and associated subtype predictors, which might facilitate the development of precision therapy for gliomas.

2. Materials and methods

2.1. Data acquisition and processing

Published bulk RNA sequencing expression and clinical information were downloaded from the University of California Santa Cruz (UCSC) Xena website (https://xenabrowser.net)[17] and the Chinese Glioma Genome Atlas (CGGA) website (http://cgga.org.cn)[18]. The expression dataset IDs were TCGA-LGG.htseq_fpkm.tsv, mRNAseq_693, and mRNAseq_325 (hereafter referred to as TCGA LGG, CGGA693, and CGGA325, respectively). FPKM (fragments per kilobase of transcript per million fragments mapped) were transformed into TPM (transcripts per million) values using the formula $TPM = \frac{FPKM}{\Sigma(FPKM)} * 10^6$. Genes detected in all three datasets were used for downstream analyses. Patients with WHO grade II and III gliomas in the datasets were included in the analysis. The TCGA LGG, CGGA693, and CGGA325 datasets contained 495, 420, and 182 samples with complete survival data, respectively, which were included in the current study. Copy number variation data of LGG patients were downloaded from the TCGA database and processed with GISTIC2.0 from the GenePattern website (https://cloud.genepattern.org/) to identify significantly amplified or deleted genomic regions[19]. An scRNA-seq dataset (GSE103224)[20] containing 17,185 cells from eight patients was downloaded from the GEO database.

2.2. mRNA stemness index derivation

A one-class logistic regression model based on pluripotent stem cell samples (embryonic and induced) from the Progenitor Cell Biology Consortium (PCBC) (SynID syn2701943) was used to calculate the mRNAsi[8,16]. Spearman correlations were calculated between the weight vector of the model and the expression profiles of the samples in the TCGA and CGGA datasets. The indices were then mapped to a range from 0 to 1 with a linear transformation that subtracted the minimum and divided by the Spearman correlation coefficient.

2.3. Functional and pathway enrichment analysis

Patients with LGG were divided into high- and low-stemness subgroups using the median of the mRNAsi. Differential analysis was performed using the Wilcoxon rank sum test with thresholds of FDR < 0.01 and $|\log2FoldChange| > 1.5$[21]. Kyoto Encyclopedia of Genes and Genomes (KEGG)[22] and Gene Ontology (GO) pathway enrichment analyses[23] were performed using the differentially expressed genes from the high and low mRNAsi subgroups using the clusterProfiler R package[24] with a p-value < 0.05. Gene set variation analysis was performed to identify signaling pathway alterations between the two mRNAsi subgroups using the GSVA R package[25].

2.4. Single-cell RNA-sequencing analysis

Single-cell RNA-seq data were processed using the Seurat(v 4.3.0) R package[26]. Cells with < 200 or > 5000 transcripts were excluded to filter out empty droplets and low-quality cells. Cells with $> 5\%$ mitochondrial genes were excluded because of poor quality[27]. The NormalizeData function in the Seurat R package was then employed to scale the raw counts in each cell to 10,000. Log transformation was also performed. The FindVariableFeatures function was used to identify highly variable genes[26,28,29]. Principal component analysis was performed with the top 2000 most variable genes identified and tSNE dimensionality reduction was performed with the top 15 principal components. Established methods and cell markers were used for cell malignancy and cell type annotation[30]. The mRNAsi of single cells was calculated using the scCancer R package[31]. Differentially expressed genes in high and low mRNAsi malignant cells were identified using the DESeq2 R package[32]. Interactions of malignant cells with immune cells were inferred using the CellChat R package.

2.5. Stemness-based classification of LGG patients

Weighted gene coexpression network analysis (WGCNA) was performed to identify the gene module most correlated with the mRNAsi. Pearson correlation coefficient between two genes from the expression data was calculated and the similarity matrix was constructed. An adjacency matrix was converted with a soft threshold of 5. The adjacency matrix was transformed into a topological matrix by the topological overlap metric (TOM). A gene dendrogram was identified by average linkage hierarchical clustering. The modules were obtained by Dynamic Tree Cut. Genes of the identified module and differentially expressed genes from the high and low mRNAsi subgroups of GSE103224 were intersected to identify genes responsible for malignant cell stemness. Multivariate Cox regression analysis was performed to construct the GSScore[33–36]. Differentially expressed genes from the high and low GSScore groups were identified using the Wilcoxon rank-sum test with thresholds of FDR < 0.01 and log2FoldChange > 1. The ConsensusClusterplus function was then used based on the differentially expressed genes from the GSScore subgroups to establish a new classification of LGG patients. Unsupervised consensus clustering was performed by resampling 80% of the data over 1000 iterations. The optimal cluster number was determined using CDF curves, the PAC algorithm, and a consensus heatmap.

2.6. Chemotherapeutic response prediction

The Tumor Immune Dysfunction and Exclusion (TIDE) algorithm [37–40] was used to predict the response of the patients to immunotherapy in each LGG cluster. The Profiling Relative Inhibition Simultaneously in Mixtures (PRISM) dataset[41] contains gene expression profiling and drug sensitivity information of different types of cancer cell lines. The CERES score[42] measures the essentiality of genes for the survival of cancer cell lines. The correlation of GSScores and glioma target genes in glioma cell lines was calculated. The OncoPredict R

package was used to predict the response of patients to chemotherapeutics, including TMZ[43]. The IC50 of LGG patients was estimated using ridge regression by integrating expression profiles from the Genomics of Drug Sensitivity in Cancer (GDSC2), Cancer Therapeutics Response Portal (CTRP2) database (https://www.cancerrxgene.org), and LGG samples[44–47]. The area under the dose response curve (AUC) is a measure of drug sensitivity, with a lower value indicating a higher sensitivity to the drug[46].

2.7. Machine learning identification of stemness subtype predictors

TCGA LGG patients were randomly divided into training and testing sets at a ratio of 7:3 using the caret R package. We then divided patients with LGG into high and low subgroups based on the median GSScore. Differentially expressed genes from the high and low GSScore subgroups were used as input for feature selection in LGG sample clustering using four machine learning methods. Boruta, support vector machine (SVM), extreme gradient boosting (XGBoost), and least absolute shrinkage and selection operator (LASSO) were used to select genes of importance. For the Boruta function, the confidence level was set to 0.01, and the maximal number of importance source runs was set to 1000. Intersections of the genes selected by the four methods were used in the multivariate logistic regression analysis to construct the stemness subtype predictor. We evaluated the performance of the stemness subtype predictor using the ROC and precision-recall curves in the training and testing sets.

2.8. Cell culture

The glioma patient-derived cell coded "GPDC8″ was generated from a patient with glioma who underwent surgical resection at the Department of Neurosurgery, Xiangya Hospital in 2020. Tumor tissues were enzymatically dissociated and cultivated in serum-free NSA culture medium, as previously described[48]. The T98G cell line was purchased from the Shanghai Cell Bank of the Chinese Academy of Sciences. Cell lines were incubated in Dulbecco's Modified Eagle Medium supplemented with 10% fetal bovine serum at 37 °C and 5% CO_2.

2.9. Drug application and cell viability assay

The cells were seeded in 96-well plates at a density of 10,000 cells/well. Dasatinib, TGX-221, and ifosfamide (Selleck Chemicals, TX, USA) were applied at different concentrations (0.1, 1, 10, 50, and 100 μmol/L for dasatinib; 0.1, 1, 10, and 50 μmol/L for TGX-221; and 0.1, 1, and 10 μmol/L for ifosfamide). Viability was measured 3 days after drug application using the Cell Counting Kit-8 (Cat. No. BA00208, Bioss, Beijing). Cell apoptosis was measured 1 day after drug application using Annexin V/FITC-PI (C1062S, Beyotime, China).

2.10. Statistical analysis

Statistical analysis was performed using R software (version 4.1.1) and GraphPad Prism6 (version 6.02). The Wilcoxon rank-sum and Kruskal—Wallis tests were used to compare continuous variables in multiple groups. Student's *t*-test was used to compare continuous variables in two groups unless otherwise declared. The Wilcoxon rank-sum test was more effective in FDR control than other methods in population-level RNA-seq studies with large sample sizes, and we used the Wilcoxon rank-sum test as appropriate[21]. The Kaplan—Meier curve and log-rank test were used to compare survival differences between the groups. Two-way analysis of variance was used to compare differences in cell lines in response to drugs (alpha=0.05). ROC curves and prediction-recall curves were used to assess the predictive value of the models.

3. Results

3.1. Associations between the stemness index and clinical features

The mRNAsi[8] was calculated using The Cancer Genome Atlas (TCGA) LGG dataset. Correlations between the mRNAsi and clinicopathological features were explored (Fig. 1**A&B**). The mRNAsi was ranked according to different clinicopathological subgroups, as shown in Fig. 1**C**. There were no significant differences in the mRNAsi among different age and sex subgroups. With regard to cellular heterogeneity, we examined the correlation of mRNAsi with four subtypes of glioma [49], of which the mesenchymal subtype was strongly associated with the cultured astroglial signature, the proneural subtype was highly enriched with the oligodendrocytic signature, the classical subtype was strongly associated with the murine astrocytic signature, and the neural subtype showed associations with oligodendrocytic and astrocytic differentiation with an additional enrichment of genes expressed by neurons. The mesenchymal subtype had the lowest mRNAsi value, followed by the classical subtype. The neural and proneural subtypes had the highest mRNAsi values, with no significant difference between the two subgroups. Samples of WHO grade II glioma exhibited higher mRNAsi levels than those of WHO grade III glioma ($p = 0.024$). Patients who survived had significantly higher mRNAsi scores than those who didn't ($p = 0.0011$). Additionally, we assessed the mRNAsi levels of groups of patients with different mutations. Patients with mutations in *IDH* and *TERT* showed significantly higher mRNAsi levels than those without ($p = 8.5e\text{-}12$ and $p = 0.0072$, respectively). Patients with ATRX mutations had significantly lower mRNAsi levels than those without ATRX mutations ($p = 0.00012$). Patients with codeletion of 1p19q ($p < 2.2e\text{-}16$) and methylation of the *MGMT* promoter ($p = 3.2e\text{-}05$) also showed significantly higher mRNAsi scores.

3.2. The mRNAsi is correlated with the overall survival of LGG patients

Patients were stratified into high and low mRNAsi subgroups based on the median mRNAsi value. The overall survival (OS) and progression-free survival (PFS) of the different mRNAsi subgroups were analyzed using Kaplan—Meier survival analysis (Fig. 2**A**). The high mRNAsi subgroup exhibited significantly longer OS ($p = 0.00061$) and PFS ($p < 0.0001$) than the low mRNAsi subgroup. Differential expression analysis was performed between the two subgroups (Fig. 2**B**) and identified 307 differentially expressed genes (Supplementary Table S1). Functional enrichment analyses were performed using the clusterProfiler R package. Biological processes, cellular components, and molecular functions identified as significantly enriched in the high mRNAsi subgroup are shown in Fig. 2**C** and included T-cell activation, leukocyte-mediated immunity, positive regulation of cytokines, synaptic membranes, collagen-containing extracellular matrix, and extracellular matrix structural constituents. KEGG pathway enrichment analysis identified pathways enriched in the high and low mRNAsi subgroups (Fig. 2**D**) including neuroactive ligand—receptor interaction, synaptic vesicle cycle, calcium signaling pathway, cytokine-receptor interaction, phagosome, etc.

Next, we compared differences in somatic mutations between the two groups and discovered that *RYR2*, *PCLO*, *CELSR1*, *CELSR3*, and *RIMBP2* had higher mutation rates in the low mRNAsi subgroup (Fig. 2**E**). Analysis of copy number variations in mRNAsi subgroups showed that the low mRNAsi subgroup had deletions in Chr 4, Chr 6, and Chr 11, and amplifications in Chr 10 (Fig. 2**F**).

3.3. Identification of stemness subtypes in LGG

We analyzed 17,185 cells from 8 cases in the current study. Dimension reduction and unsupervised clustering were performed. Principal component analysis was applied to reduce total dimensionality (Fig. 3**A**). The t-Distributed Stochastic Neighbor Embedding (tSNE)

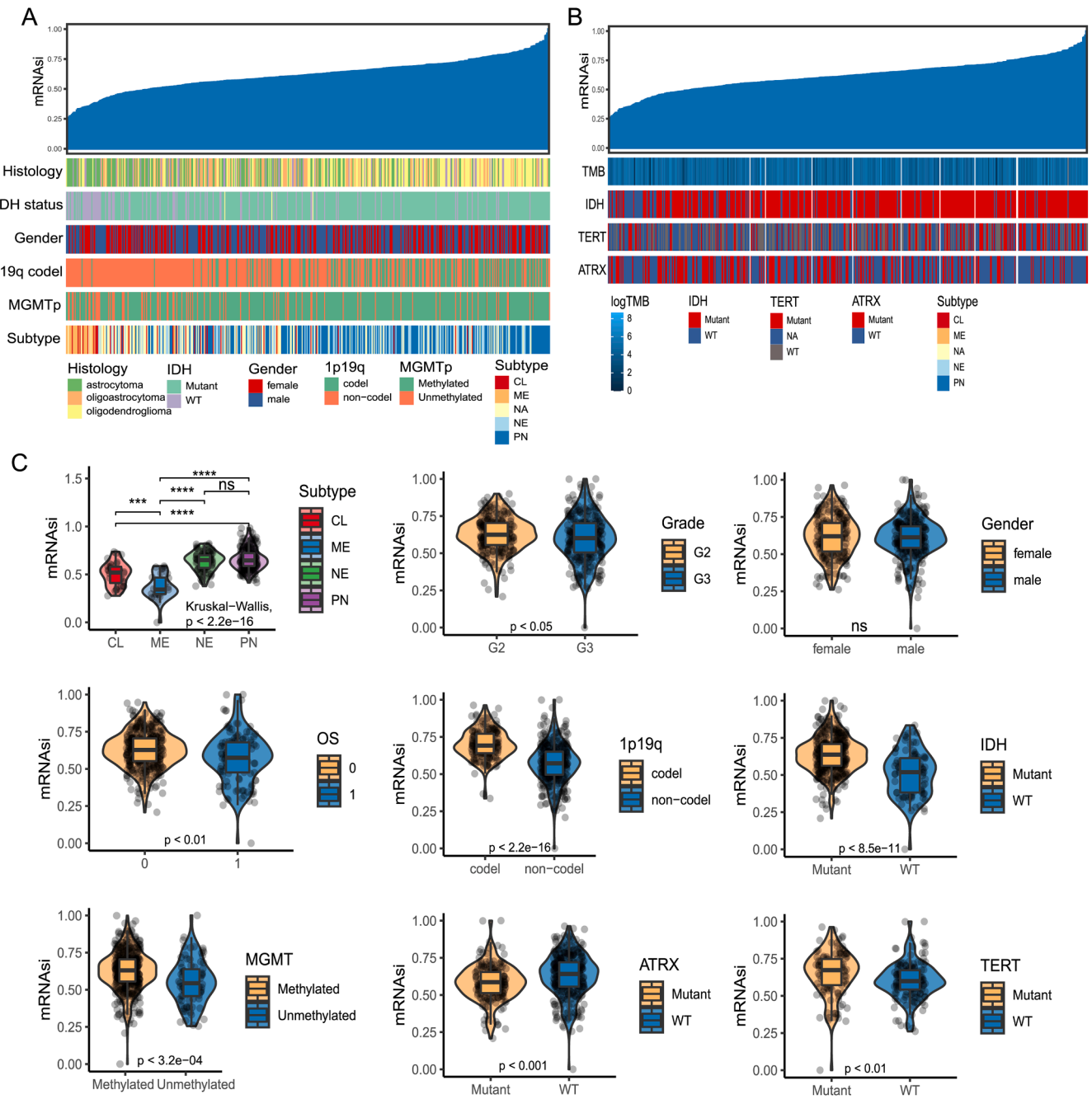

Fig. 1. The mRNA stemness index (mRNAsi) distribution in different clinicopathological groups. (A) mRNAsi correlation with different clinicopathological features. (B) mRNAsi correlation with tumor mutation burden and different gene mutations. (C) mRNAsi distribution in different clinicopathological groups. *** $p < 0.001$, **** $p < 0.0001$.

analysis identified 19 clusters of single cells (Fig. 3**B**). We annotated the clusters with cell markers validated by other studies[30] (Fig. 3**C&D**). The mRNA stemness indices of LGG malignant single cells were calculated with the scCancer R package[31] (Fig. 3**E**). Differential analysis was performed between groups of malignant cells with high and low mRNAsi levels. We also identified *IL6*, *SPP1*, and *VEGF* signaling pathways that showed significant differences in associations between high/low mRNAsi cells and monocytes/macrophages or endothelial cells (Fig. 3**F**). Weighted gene coexpression network analysis (WGCNA) identified 19 gene modules that were significantly correlated with the mRNA stemness index, among which the black module showed the highest correlation coefficient (cor = 0.72, p = 7e-67. Fig. 3**G&H**). Genes in the black module (411 genes, Supplementary Table S2) and those identified in the differential analysis (456 genes, Supplementary Table S3) (Fig. 3**I**) were intersected to acquire the three genes most correlated with the mRNAsi including *ITGB4*, *FDPS*, and *RRAS*. *ITGB4* is indicated to promote glioma stem cell self-renewal and gliomagenesis through a positive feedback loop[50]. These genes may be responsible for the stemness index of malignant cells. The GSScores were calculated using the two genes *ITGB4* and *FDPS* identified by multivariate Cox regression analysis of the three genes. $GSScore = 0.001995 * expression(ITGB4) - 0.010649 * expression(FDPS)$. GSScore was used to divide the data into high and low GSScore subgroups. Differential expression analysis identified 90 genes with differential expression between the high and low GSScore subgroups (FDR < 0.01 , $|\log2FoldChange| > 2$).

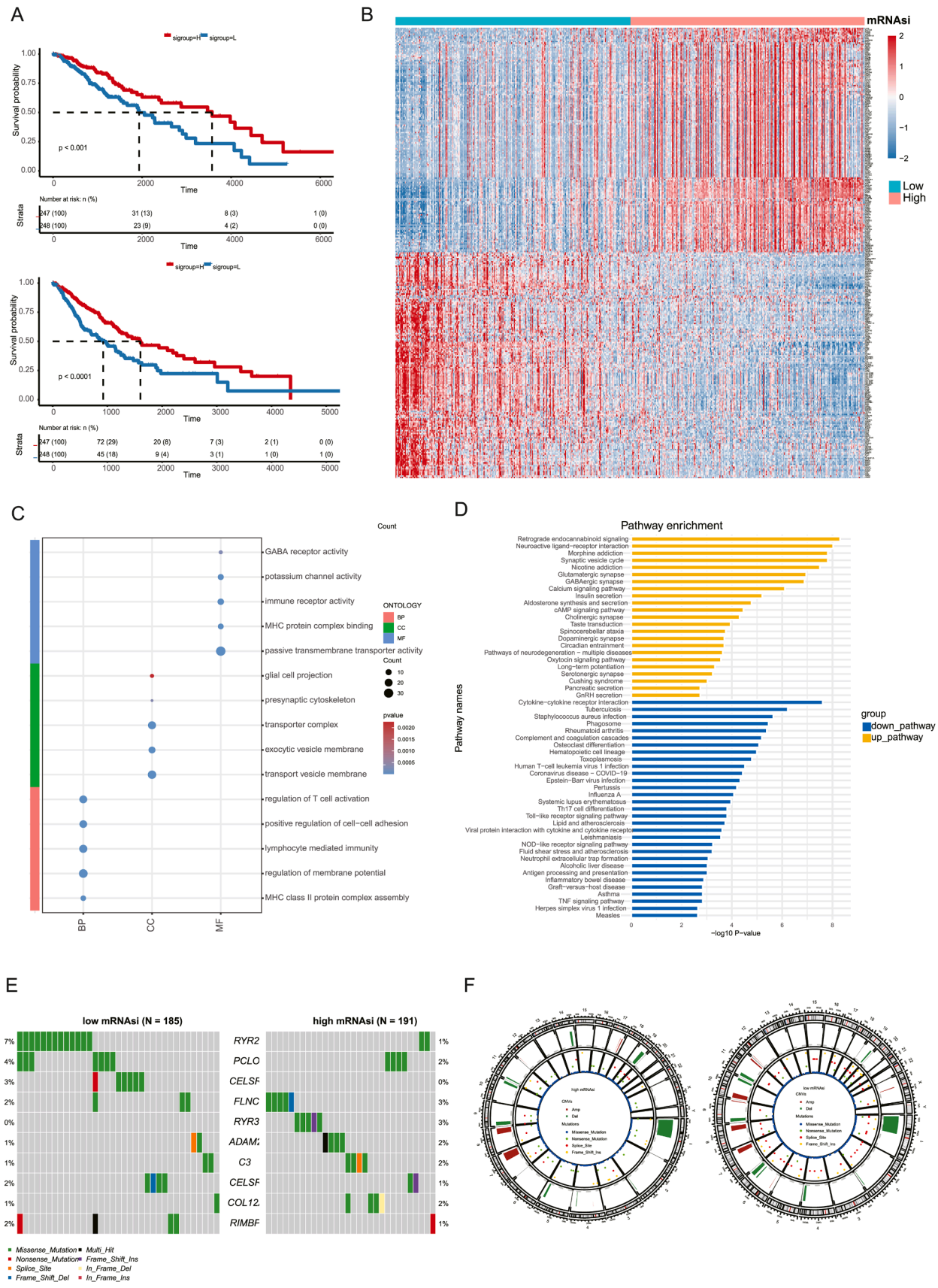

Fig. 2. Different clinical features of mRNAsi high and low groups. (A) High mRNAsi group showed significantly better OS (upper) and PFS (lower) than low mRNAsi group. (B) Heatmap of 307 differentially expressed genes between mRNAsi high and low groups. (C) GO analysis identified biological processes, cellular components, and molecular functions in DEGs of mRNAsi high and low groups. (D) KEGG analysis identified pathways differentially enriched between mRNAsi high and low groups. (E) Mutated genes different between mRNAsi high and low groups. (F) CNVs and mutations of DEGs in mRNAsi high and low groups.

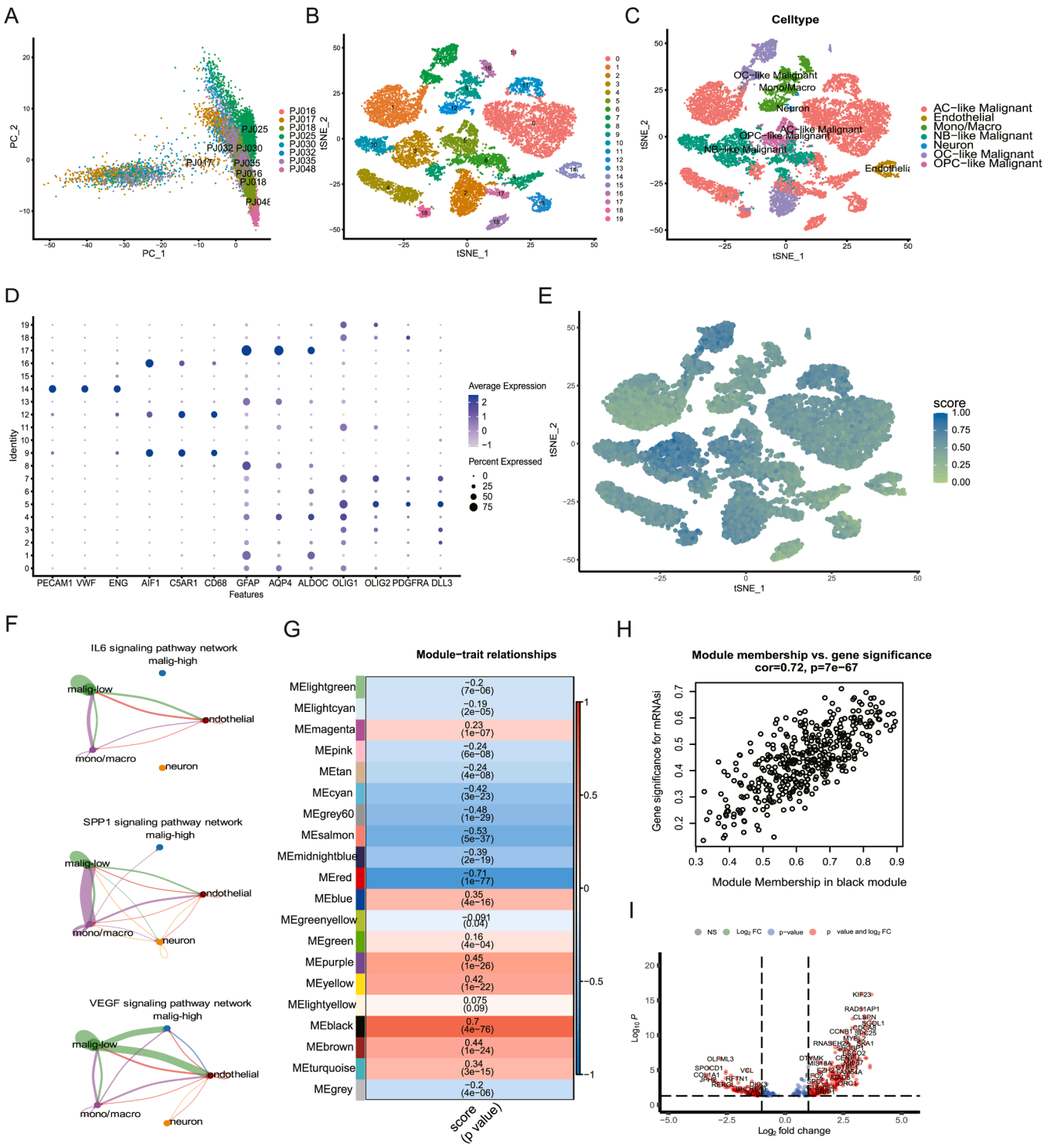

Fig. 3. Identification of differentially expressed genes between high and low GSScore subgroups. (A) Principal component analysis plot of GSE103224 dataset. (B) tSNE plot of GSE103224 dataset showing 19 clusters. (C) Cell annotations of GSE103224 with established markers. (D) Cell markers expression in different clusters. (E) mRNAsi distribution in single cells of GSE103224. (F) Differential cell communications of mRNAsi high and low malignant cells with glioma microenvironment compartments. (G) Heatmap of the correlation between mRNAsi and module eigengenes identified with WGCNA. (H) Correlation of genes in black module with mRNAsi. (I) Differentially expressed genes identified between GSScore high and low groups.

Unsupervised consensus clustering using the expression profiles of the 90 differentially expressed genes identified a new cluster of LGG patients. The consensus heatmap, relative change in the area under the cumulative distribution function (CDF) curve, and proportion of ambiguously clustering (PAC) algorithm suggested that the optimal number of clusters was three (Fig. 4**A-D**). Patients with LGG were thus clustered into three groups: Cluster 1 (C1), Cluster 2 (C2), and Cluster 3 (C3). Kaplan-Meier analysis revealed that the three clusters had significantly different OS times, with Cluster 1 showing the shortest and Cluster 3 the longest ($p < 0.0001$) (Fig. 4**E**). Pearson's correlation analysis identified a negative correlation between GSScore and mRNAsi (Fig. 4**F**). Gene set variation analysis identified gene sets that were

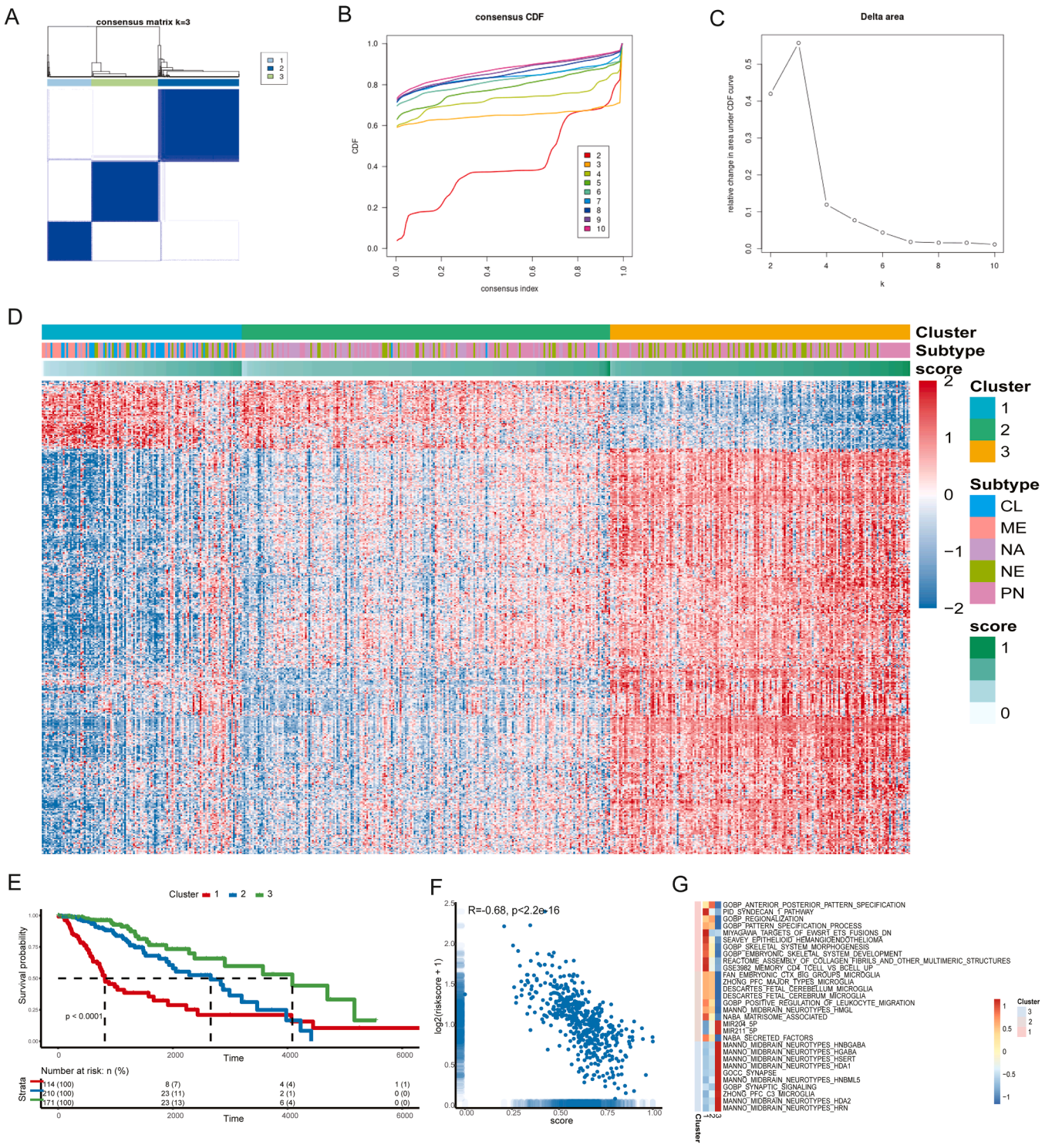

Fig. 4. Identification of three LGG stemness clusters. (A) Consensus clustering matrix for k = 3. (B) CDF curves of the consensus score from k = 2–10. (C) The relative change in the area under the curve of CDF from k = 2–10. (D) Heatmap of DEGs between the three clusters. (E) OSs of these three clusters are significantly different. (F) Correlation of GSScore and mRNAsi (r = −0.68, p < 2.2e-16). (G) GSVA analysis identified differentially enriched cell type signatures among the three clusters.

enriched in the three clusters (Fig. 4**G**). C1 mainly comprises the classical and mesenchymal subtypes, while C2 and C3 mostly comprise the proneural and neural subtypes. The GSVA analysis shows C1 enrichment of epithelial mesenchymal transition and hypoxia pathways and C3 enrichment of synaptic and neurotransmitter associated pathways. The significant differences in survival time, subtype composition, and pathway enrichment of the three clusters might indicate some common biological characteristics in each of the clusters.

3.4. Stemness subtypes exhibit different clinicopathological characteristics

Clinicopathological patterns differed among the three stemness subtypes. The mRNAsi was significantly different among the three clusters, with C1 having the lowest and C3 showing the highest mRNAsi scores (p < 2.2e-16). The GSScores of C1 and C2 were significantly higher than that of C3 (p < 2.2e-16). C2 included younger patients, whereas C3 included elderly patients (p = 4.4e-12) (Fig. 5**A**). The

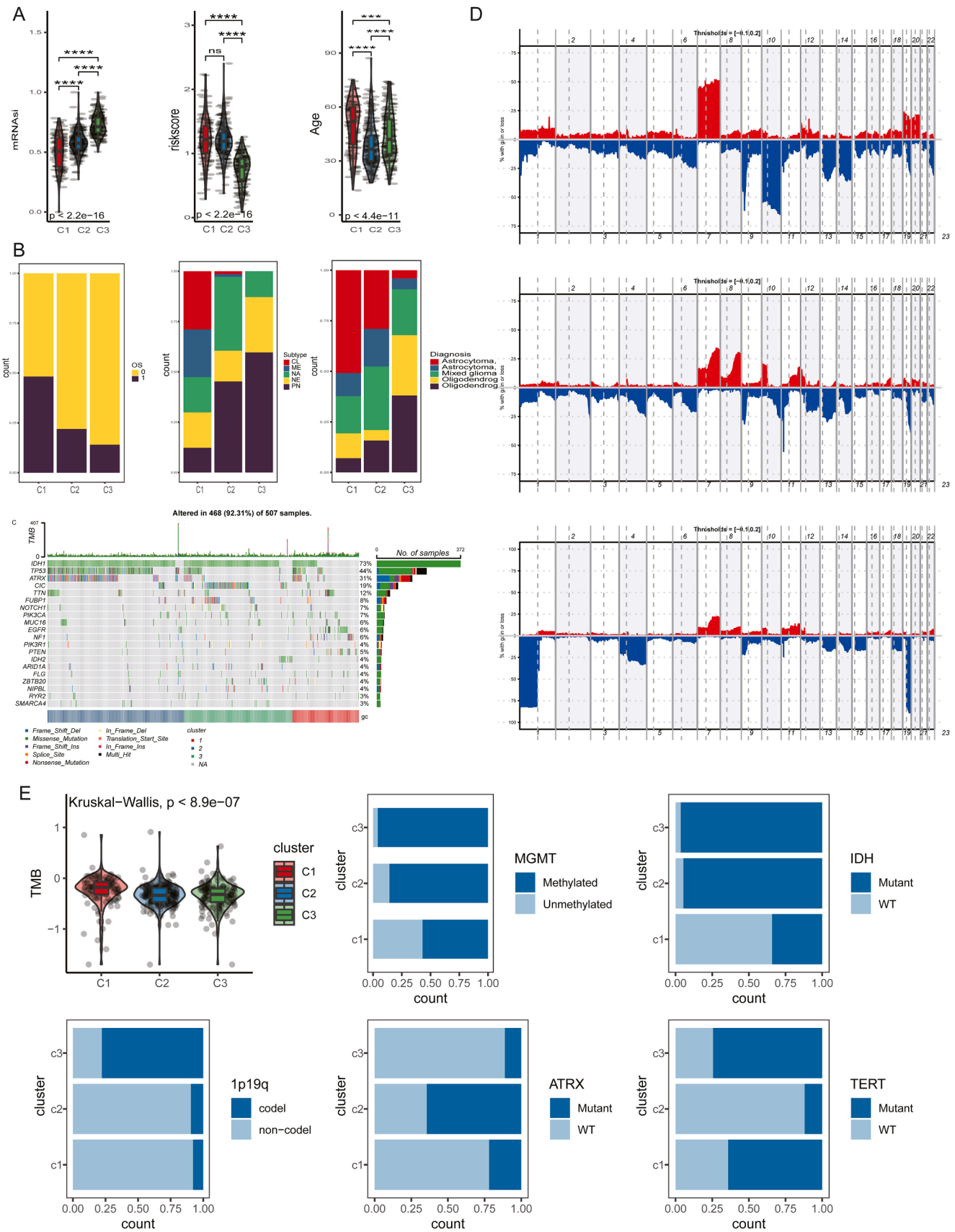

Fig. 5. Clinicopathological features of three LGG stemness clusters. (A) mRNAsi, GSScore, and age distribution in the three LGG clusters. (B) Survival status, subtype, pathology diagnosis distribution in the three LGG clusters. (C) Mutations in the three clusters. (D) CNVs in the three clusters. (E) TMB, MGMT, IDH, ATRX, TERT mutation and 1p19q codeletion status in the three clusters.

distributions of OS time, molecular subtype, and pathological diagnosis were also different among the clusters (Fig. 5**B**). Nearly half of the C1 patients and less than a quarter of the C2 and C3 patients were deceased. The proneural subtype accounted for half of the C2 and C3 patients, whereas the classical subtype was primarily observed in C1. Somatic mutations were also differentially distributed in the three clusters, with IDH1 mutations primarily observed in C2 and C3; TP53 and ATRX mutations primarily observed in C2 CIC and FUBP1 mutations primarily observed in C3; and EGFR and PTEN mutations primarily observed in C1 (Fig. 5**C**). Copy number variation analysis revealed a significant increase in Chr 7 and loss of Chr 10 in C1 and a significant loss of Chr 1p and Chr 19q in C3 (Fig. 5**D**). The tumor mutation burden was significantly different among the three clusters ($p = 8.9e\text{-}08$) (Fig. 5**E**). Unmethylated MGMT was primarily detected in C1.

3.5. Stemness subtypes harbor distinct tumor immune microenvironment (TIME) and immunogenomic patterns

The tumor immune score, stromal score, and tumor purity were calculated using the ESTIMATE algorithm (Fig. 6**A**). Immune ($p = 4.1e\text{-}13$) and stromal ($p = 4.7e\text{-}09$) scores were significantly higher in C1 and C2 than in C3. Tumor purity was significantly higher in C3 than in C2 and C1 ($p = 4.5e\text{-}05$). CIBERSORT was used to identify the proportion of immune cells in the three clusters (Fig. 6**B**). Among all TIME component cells, M2 macrophages, monocytes, resting CD4 memory T cells, and activated NK cells showed the highest infiltration rates in LGG. Infiltration by M2 macrophages, resting CD4 memory T cells, M1 macrophages, regulatory T cells, and CD8 T cells was significantly higher in C1 than in C2 and C3. The infiltration of monocytes, activated NK cells, and activated mast cells was significantly higher in C2 than in C1 and C3. Naïve CD4 T cells and follicular helper T cells exhibited significantly higher infiltration rates in C3 than in C1 or C2. PD1/PDL1/PDL2 and CTLA4/CD80/CD86 expression levels were consistently highest in C1 and were higher in C2 than in C3 (Fig. 6**C**). The tumor immune dysfunction and exclusion (TIDE) algorithm was then used to predict the response of patients with LGG to immunotherapy. C2 patients experienced the highest response rate to immunotherapy among the three clusters (Fig. 6**D**). The correlation between immunotherapy response and GSScore was also explored; patients responding to immunotherapy tended to have higher GSScores (Fig. 6**E**). The IC50 of TMZ was estimated in the three clusters, demonstrating that C1 and C3 had significantly lower IC50 values than C2 ($p < 2.2e\text{-}16$) (Fig. 6**F**).

3.6. Machine learning construction and validation of stemness subtype predictors

Four machine learning algorithms, namely, Boruta, support vector machine (SVM), extreme gradient boosting (XGBoost), and least absolute shrinkage and selection operator (LASSO), were used to identify genes critical for stemness subtype prediction. Boruta, SVM, XGBoost, and Lasso identified 152, 17, 70, and 40 genes, respectively (Fig. 7**A**). Seven genes, including TNNT1, KCNH7, CHI3L1, SPOCD1, ITGB4, XKR7, and TRIM67, commonly identified by the four algorithms were used to construct a stemness subtype predictor using multivariate logistic regression analysis. TNNT1 has been identified as a potential vulnerability or biomarker in diffuse midline glioma[51]. KCNH7 mutation is associated with poor survival in esophageal squamous cell carcinoma[52]. CHI3L1 modulates immune suppression in glioblastoma [53] and promotes glioma progression[54]. SPOCD1 is upregulated as a transcription factor in glioblastoma[55]. ITGB4 is indicated to promote glioma stem cell self-renewal and gliomagenesis through a positive feedback loop[50]. TRIM67 upregulation induces the blebbing morphology of cells, higher cell motility and reduced cell adherence, contributing to gliomagenesis[56]. The confusion matrix, receiver operating characteristic (ROC), and precision-recall curves were used to evaluate the performance of the subtype predictor in the training (Fig. 7**B&C**) and testing datasets (Fig. 7**D&E**). The accuracies of the subtype predictor in the training and testing sets were 0.983 and 0.905, respectively. The subtype predictor performed well in clustering samples of CGGA693 and CGGA325 datasets into three clusters with differential prognoses (accuracy for CGGA693 and CGGA325 was 0.878 and 0.801, respectively). The expression levels of the seven genes in the two datasets were consistent, as shown in Fig. 7**F&H**. The OS of the three clusters was evaluated using Kaplan–Meier plots, which revealed that the OS of C1 patients was significantly shorter than that of C2 and C3 patients (Fig. 7**G&I**).

3.7. GSScores predict drug targets and chemotherapeutics

Correlation analysis was performed between drug targets from the literature[57] and the GSScore to identify potential therapeutic targets with correlation coefficients higher than 0.4 and $p < 0.05$ (Fig. 8**A**). The CERES method estimates gene-dependency levels from CRISPR—Cas9 essentiality screens while accounting for the copy number-specific effect. The correlation between the CERES score of drug targets and the GSScore was then calculated to find targets indispensable for cell growth (Fig. 8**B**). We hypothesize that the genes identified in this analysis represent putative targets in patients with high GSScores; therapies targeting these genes may provide beneficial outcomes for patients.

Drugs with lower area under the curve (AUC) values in the high GSScore subgroup were identified with differential analysis. The Genomics of Drug Sensitivity in Cancer (GDSC2) and Cancer Therapeutics Response Portal (CTRP2) drug response datasets were used to identify candidate drugs that showed significantly lower AUC values in the high GSScore subgroup. Dasatinib was identified in the GDSC2 dataset as having a correlation between the AUC and GSScore < -0.4, while ifosfamide, TGX-221, IC-87114, and fumonisin B1 were similarly identified in the CTRP2 dataset (Fig. 8**C&D**). Candidate drugs and their corresponding targets were analyzed to identify promising target pathways for the high GSScore subgroup. TCR, Wnt, and RTK signaling were identified as putative target pathways for the treatment of patients with high GSScores (Fig. 8**E**). We further validated the performance of the predicted drugs in vitro using GPDC8 cells with stem-like characteristics and T98G glioma cells. Dasatinib, TGX-221, and ifosfamide exhibited higher sensitivity in GPDC8 cells than in T98G cells in drug sensitivity experiments (Fig. 8**F**). GPDC8 also showed higher apoptosis rates than T98G when treated with dasatinib, TGX-221, or ifosfamide (Fig. 8**G**). Drug response was compared between a cell line lacking stemness (T98G) and a corresponding cell line showing high sphere forming abilities (GPDC8). As the drugs tested were predicted to be more sensitive to cells with high stemness, the results showing lower cell viability in GDPC8 cells than in T98G cells treated with the same concentrations of a drug showed the validity of the GSScore in the prediction of drug responses, providing novel insights into precision medicine for LGG treatment.

4. Discussion

In this study, we analyzed the correlation between LGG stemness and clinicopathological characteristics. We derived a machine learning-based method to distinguish LGG subtypes. The three subtypes identified were significantly correlated with patient prognosis. We further validated its correlation with patient prognosis in CGGA datasets. We also derived a GSScore and validated its performance in predicting drug responses.

GSCs can preserve a special TME niche comprising immunocytes, arterioles, endothelial cells, pericytes, and other components[12,58,59]. GSCs recruit M2 macrophages and induce Treg cell expansion to suppress immune responses. Direct contact between GSCs and immunocytes can induce the inhibition of immune cell function via PD-L1 mediation [60]. Pathways identified in the high mRNAsi subgroup included T cell activation, leucocyte-mediated immunity, positive regulation of

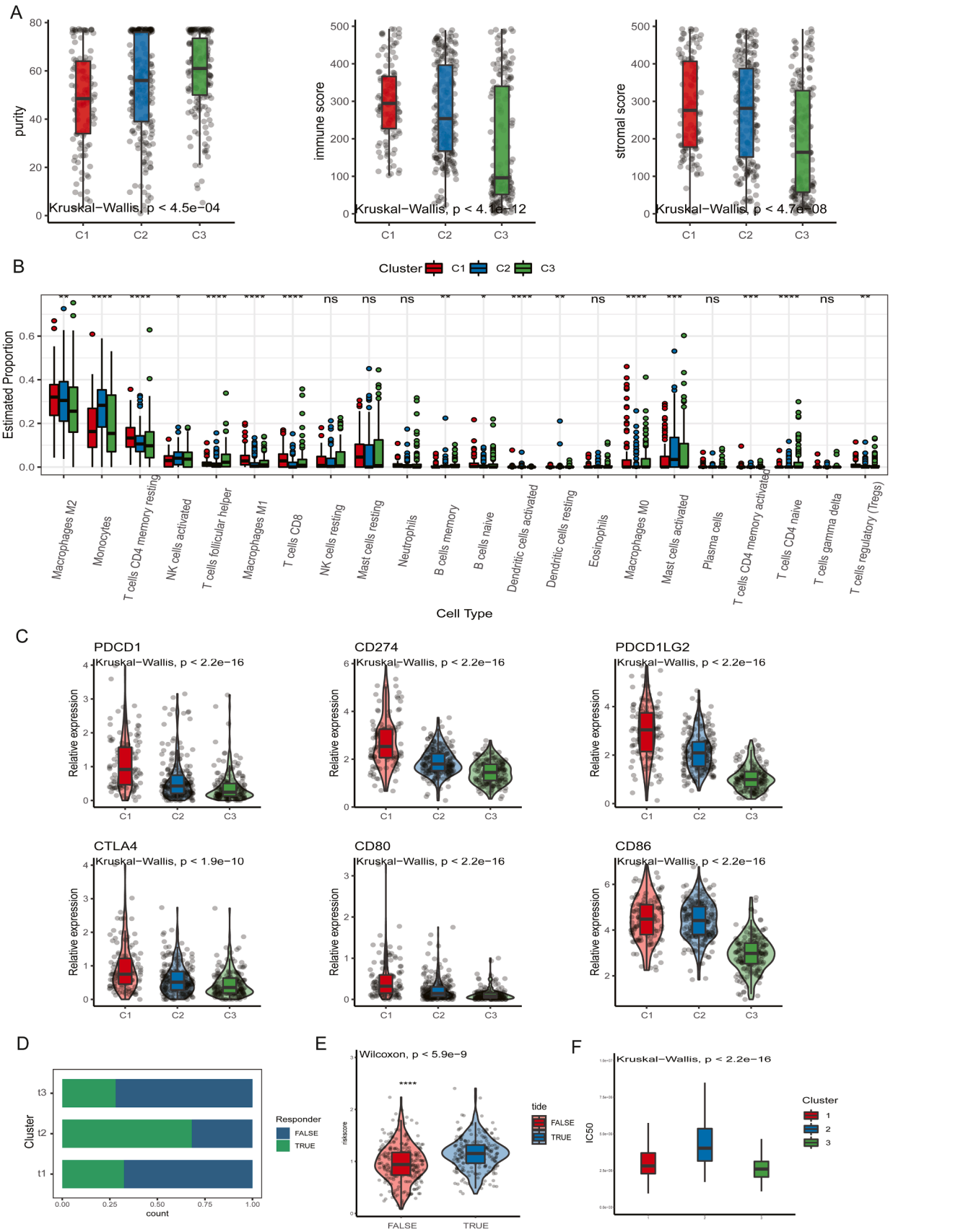

Fig. 6. Immune characteristics of three LGG stemness clusters. (A) Tumor purity, immune score, stromal score distribution of three LGG clusters. (B) Immune cell infiltration of three LGG stemness clusters. (C) Immune checkpoints expression of three LGG stemness clusters. (D) Proportions of responders and non-responders of immunotherapy in LGG stemness clusters. (E) GSScores of responders and non-responders to immunotherapy. (F) Different IC50 value of temozolomide in three LGG stemness clusters.

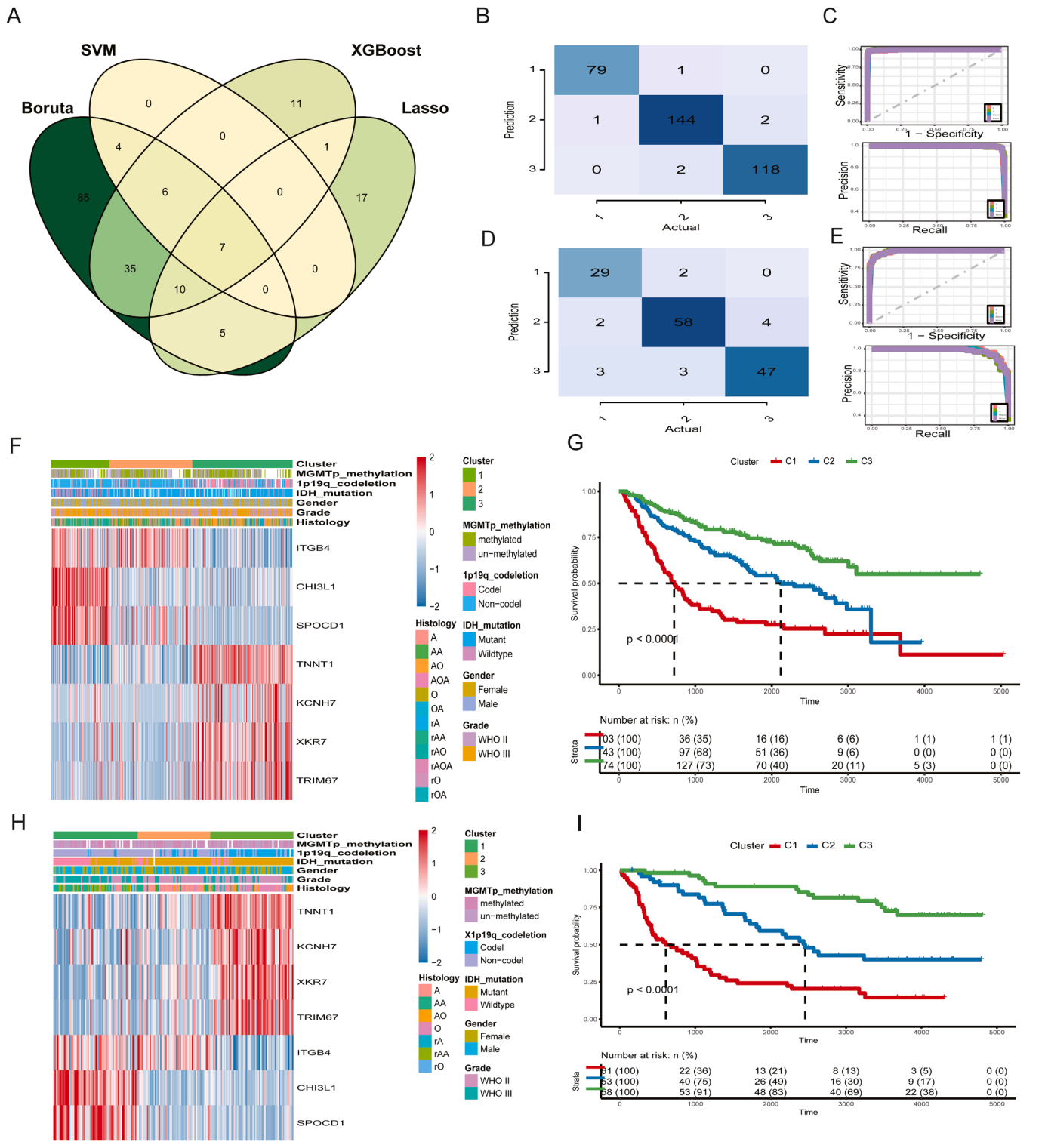

Fig. 7. Construction and validation of stemness subtype predictor. (A) Venn diagram showing seven genes identified by four machine learning methods. (B) Confusion matrix of stemness subtype predictor for the training set. (C) ROC curve and prediction-recall curve of stemness subtype predictor for the training set. (D) Confusion matrix of stemness subtype predictor for the testing set. (E) ROC curve and prediction-recall curve of stemness subtype predictor for the testing set. (F) Heatmap showing the stemness subtype predictor components expression in CGGA693 dataset. (G) Kaplain-Meier curve showing overall survival in different stemness subtypes in CGGA693 dataset. (H) Heatmap showing the stemness subtype predictor components expression in CGGA325 dataset. (I) Kaplain-Meier curve showing overall survival in different stemness subtypes in CGGA325 dataset.

cytokines, synaptic membranes, collagen-containing extracellular matrix, and extracellular matrix structural constituents. These results substantiate past findings of GSC recruitment and interactions with macrophages and T cells[61–63]. The current study identified high expression of multiple immune checkpoints in C1 patients, which exhibited the worst prognosis and harbored the highest M2 infiltration, corroborating a correlation between stemness and immune suppression. Multiple pathways, including the IL6, SPP1, and VEGF signaling

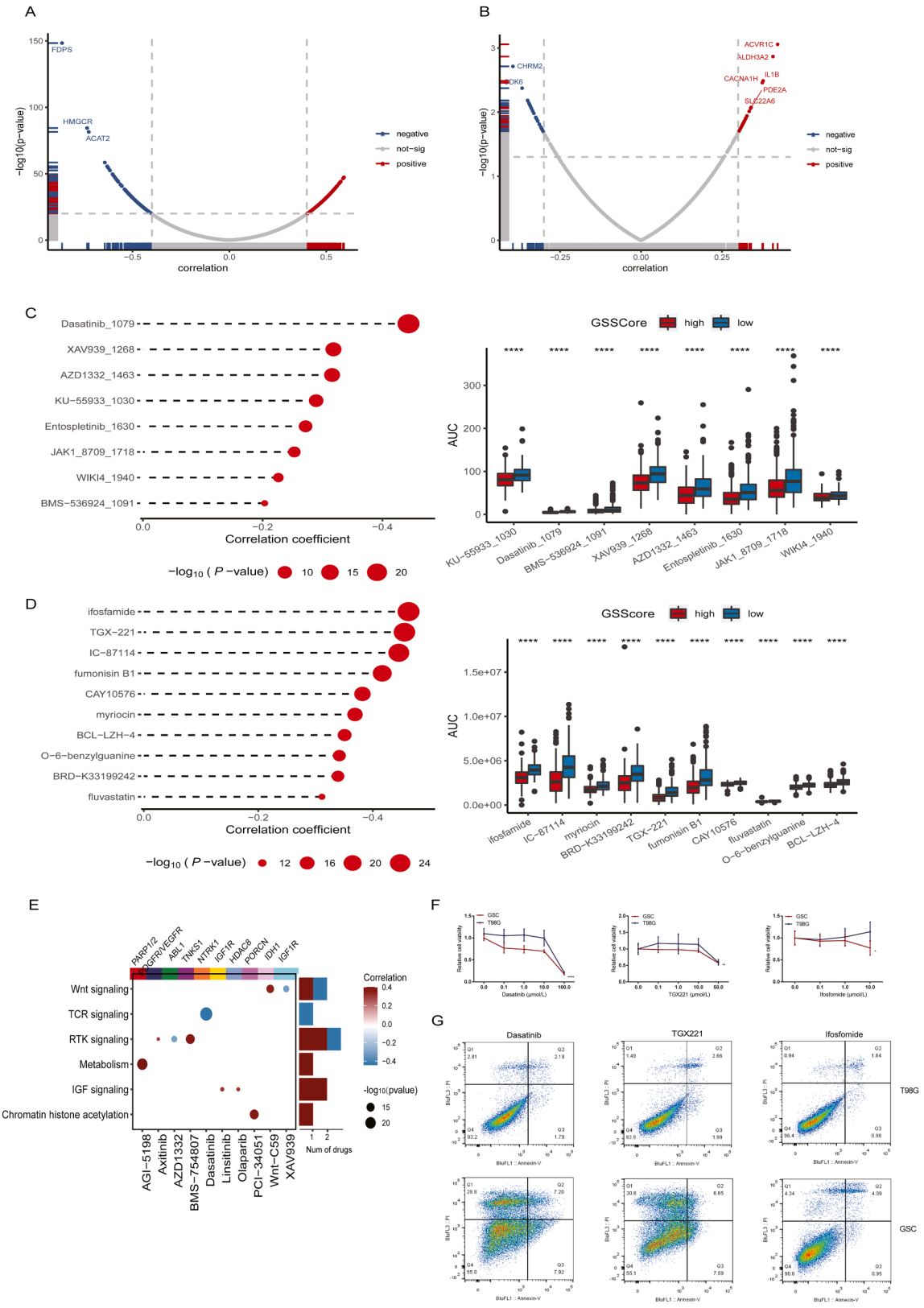

Fig. 8. GSScore correlations with and prediction of chemotherapeutic drugs. (A) Spearman correlation between drug targets and the GSScore. (B) Spearman correlation between drug target CERES scores and the GSScore. (C&D) GDSC2 and CTRP2 related compounds identified with a negative correlation between the GSScore and AUC value. (E) Correlation of drug sensitivity with the GSScore and corresponding drug targets and associated pathways in GDSC2 dataset. (F) Dose-response curves of glioma spheroid forming cells GPDC8 and glioma cells T98G treated with dasatinib, TGX-221, and ifosfomide. (G) Cell apoptosis rates of T98G cells were significantly lower than GPDC8 stem-like cells when treated with Dasatinib, TGX221, or Ifosfamide at the same concentrations.

pathways, were identified to be differentially activated in the interactions of high and low GSScore malignant cells with monocytes/macrophages or endothelial cells. These pathways may be worth studying to further understand the interactions of GSCs with the glioma TME[64–66].

The failure of cancer treatment can be ascribed to metastasis, recurrence, heterogeneity, resistance to chemotherapy and radiotherapy, and immunological approaches in which CSCs are essential agents[67]. In addition, many subtypes of GSCs have different characteristics and exhibit complicated responses to therapies, particularly chemotherapy. TMZ is currently used as a front-line chemotherapeutic agent to treat gliomas[68]. The effectiveness of TMZ varies significantly in in-vitro experiments and in the TME[48]. Another study indicated that TMZ preferentially depletes GSCs but not the entire population[69]. The differences in responses to TMZ in the three clusters identified in this study implied differences in stemness. Further research should be conducted to explore the mechanisms underlying TMZ responses as they relate to stemness.

Serpin peptidase inhibitor clade H member 1 was found to be highly predictive of dasatinib response[70] in glioma. Although dasatinib, as an SRC inhibitor, has failed in clinical trials of recurrent glioblastoma patients to improve overall survival[71], the current study may provide a new angle for dasatinib response improvement through patient stratification. TGX-221 selectively blocks p110beta of the phosphatidylinositol 3-kinase pathway. It has been proven to significantly decrease tumor growth in nude mice and transgenic mouse models of prostate cancer[72,73]. A study also showed an inhibition of proliferation in human glioblastoma cells[74]. Our study corroborates TGX221 in its possible role in glioma treatment. Ifosfamide has been utilized in combination with other drugs to treat recurrent glioblastoma and has proven to be an option for patients[75]. The current study may provide a new perspective for patient selection in ifosfamide treatment of glioma patients.

This study has some limitations. The validation test was performed only on the CGGA datasets, and validation of clinic-derived data is needed. Examination of the subtypes at the single-cell level may provide additional insights. The correlation of the subtypes and GSScores with immunotherapy is not discussed in the current manuscript and requires more attention in future studies.

5. Conclusions

In this study, LGGs were classified into three subtypes with low, medium, and high stemness indices. The subtypes showed significantly different prognoses and immune cell infiltrations. Subtype predictors were identified using machine-learning methods and performed well in the validation datasets. Our finding that the GSScore was negatively correlated with the stemness index and predicted drug responses provides a promising method for clinical drug screening.

Ethics approval and consent to participate

Informed consent was obtained from all the patients before the study. This study was approved by the Ethics Committee of Xiangya Hospital, Central South University (registration number: ChiCTR2100047049; ethics approval number: 201703478).

Authors' contributions

Zhou HS, Zhang LY, and Li CT designed and drafted the manuscript. Zhou HS, Zhang LY, Li CT and Chen B organized the figures and edited the legends. Chen B, Zhang LY and Li CT revised the article. Zhou HS, Zhang LY, and Li CT conducted the data analysis. Zhang LY generated GPDCs. All authors have read and approved the final manuscript.

Simple summary

Glioma is the most common primary malignancy of the central nervous system. Lower-grade gliomas present highly variable clinical outcomes. In this study, we aimed to investigate new clustering of lower grade gliomas with a one-class logistic regression model and identify predictors of LGG clustering. We calculated the mRNA stemness index in bulk and single-cell RNA-sequencing datasets and investigated the correlation between stemness and clinicopathological characteristics. A glioma stemness-associated score (GSScore) was constructed using multivariate Cox regression analysis and validated to predict chemotherapeutic responses in glioma cell lines. We also utilized the GSScore to cluster LGG samples into three stemness subtypes. Differences in clinicopathological characteristics among the three stemness-associated subtypes were identified. We further identified seven genes as subtype predictors using machine learning methods and validated their performance with public datasets.

Funding

This work was supported by the Natural Science Foundation of China (no. 81402249 to L.Y. Zhang), Natural Science Foundation of Hunan Province (no. 2019JJ50963 to L.Y. Zhang and no. 2023JJ30897 to C.T. Li)

CRediT authorship contribution statement

Hongshu Zhou: Conceptualization, Methodology, Formal analysis, Writing – original draft, Visualization. **Bo Chen:** Formal analysis, Validation, Writing – original draft. **Liyang Zhang:** Conceptualization, Methodology, Funding acquisition. **Chuntao Li:** Conceptualization, Methodology, Supervision, Project administration, Funding acquisition, Writing - review & editing.

Declaration of Competing Interest

All authors declare that they have no conflict of interest.

Data Availability

The data for bioinformatic analysis are available in the open-source TCGA, GEO, and CGGA databases.

Appendix A. Supporting information

Supplementary data associated with this article can be found in the online version at doi:10.1016/j.csbj.2023.07.029.

References

[1] Weller M, et al. Glioma. Nat Rev Dis Prim 2015;1:15017.
[2] Molinaro AM, et al. Genetic and molecular epidemiology of adult diffuse glioma. Nat Rev Neurol 2019;15(7):405–17.
[3] Reifenberger G, et al. Advances in the molecular genetics of gliomas - implications for classification and therapy. Nat Rev Clin Oncol 2017;14(7):434–52.
[4] Chen, B., et al., *Glioma stem cell signature predicts the prognosis and the response to tumor treating fields treatment.* CNS Neurosci Ther, 2022.
[5] Yang K, et al. Glioma targeted therapy: insight into future of molecular approaches. Mol Cancer 2022;21(1):39.
[6] Teng C, et al. Recurrence- and malignant progression-associated biomarkers in low-grade gliomas and their roles in immunotherapy. Front Immunol 2022;13:899710.
[7] Brat DJ, et al. Comprehensive, integrative genomic analysis of diffuse lower-grade gliomas. N Engl J Med 2015;372(26):2481–98.
[8] Malta TM, et al. Machine learning identifies stemness features associated with oncogenic dedifferentiation. Cell 2018;173(2):338–54. e15.
[9] Prieto-Vila M, et al. Drug resistance driven by cancer stem cells and their niche. Int J Mol Sci 2017;18(12).
[10] Smits M, van den Bent MJ. Imaging correlates of adult glioma genotypes. Radiology 2017;284(2):316–31.
[11] Suvà ML, Tirosh I. The glioma stem cell model in the era of single-cell genomics. Cancer Cell 2020;37(5):630–6.

[12] Wang Z, et al. The adaptive transition of glioblastoma stem cells and its implications on treatments. Signal Transduct Target Ther 2021;6(1):124.
[13] Graeber MB. Changing face of microglia. Science 2010;330(6005):783–8.
[14] Wang X, et al. Reciprocal signaling between glioblastoma stem cells and differentiated tumor cells promotes malignant progression. Cell Stem Cell 2018;22(4):514–28. e5.
[15] Schiffer D, et al. Glioblastoma niches: from the concept to the phenotypical reality. Neurol Sci 2018;39(7):1161–8.
[16] Salomonis N, et al. Integrated genomic analysis of diverse induced pluripotent stem cells from the progenitor cell biology consortium. Stem Cell Rep 2016;7(1):110–25.
[17] Goldman MJ, et al. Visualizing and interpreting cancer genomics data via the Xena platform. Nat Biotechnol 2020;38(6):675–8.
[18] Zhao Z, et al. Chinese glioma genome atlas (CGGA): a comprehensive resource with functional genomic data from chinese glioma patients. Genom Proteom Bioinforma 2021;19(1):1–12.
[19] Mermel CH, et al. GISTIC2.0 facilitates sensitive and confident localization of the targets of focal somatic copy-number alteration in human cancers. Genome Biol 2011;12(4):R41.
[20] Yuan J, et al. Single-cell transcriptome analysis of lineage diversity in high-grade glioma. Genome Med 2018;10(1):57.
[21] Li Y, et al. Exaggerated false positives by popular differential expression methods when analyzing human population samples. Genome Biol 2022;23(1):79.
[22] Kanehisa M, et al. KEGG as a reference resource for gene and protein annotation. Nucleic Acids Res 2016;44(D1):D457–62.
[23] *Gene Ontology Consortium: going forward.* Nucleic Acids Res, 2015. **43**(Database issue): p. D1049-D1056.
[24] Yu G, et al. clusterProfiler: an R package for comparing biological themes among gene clusters. Omics 2012;16(5):284–7.
[25] Hänzelmann S, Castelo R, Guinney J. GSVA: gene set variation analysis for microarray and RNA-seq data. BMC Bioinforma 2013;14:7.
[26] Stuart T, et al. Comprehensive integration of single-cell data. Cell 2019;177(7):1888–902. e21.
[27] Ochocka N, et al. Single-cell RNA sequencing reveals functional heterogeneity of glioma-associated brain macrophages. Nat Commun 2021;12(1):1151.
[28] Armaka M, et al. Single-cell multimodal analysis identifies common regulatory programs in synovial fibroblasts of rheumatoid arthritis patients and modeled TNF-driven arthritis. Genome Med 2022;14(1):78.
[29] Yao J, et al. Single-cell RNA-Seq reveals the promoting role of ferroptosis tendency during lung adenocarcinoma EMT progression. Front Cell Dev Biol 2021;9:822315.
[30] Sun D, et al. TISCH: a comprehensive web resource enabling interactive single-cell transcriptome visualization of tumor microenvironment. Nucleic Acids Res 2021;49(D1). D1420-d1430.
[31] Guo W, et al. scCancer: a package for automated processing of single-cell RNA-seq data in cancer. Brief Bioinform 2021;22(3).
[32] Love MI, Huber W, Anders S. Moderated estimation of fold change and dispersion for RNA-seq data with DESeq2. Genome Biol 2014;15(12):550.
[33] Zhang Y, et al. Identification of new head and neck squamous cell carcinoma subtypes and development of a novel score system (PGSscore) based on variations in pathway activity between tumor and adjacent non-tumor samples. Comput Struct Biotechnol J 2022;20:4786–805.
[34] Liu J, et al. Pyroptosis-related gene expression patterns and corresponding tumor microenvironment infiltration characterization in ovarian cancer. Comput Struct Biotechnol J 2022;20:5440–52.
[35] Wang Q, et al. A pathway-based mutation signature to predict the clinical outcomes and response to CTLA-4 inhibitors in melanoma. Comput Struct Biotechnol J 2023;21:2536–46.
[36] Long F, et al. Dynamic gene screening enabled identification of a 10-gene panel for early detection and progression assessment of gastric cancer. Comput Struct Biotechnol J 2023;21:677–87.
[37] Wu J, et al. A risk model developed based on tumor microenvironment predicts overall survival and associates with tumor immunity of patients with lung adenocarcinoma. Oncogene 2021;40(26):4413–24.
[38] Xu S, et al. Hypoxia-related lncRNA correlates with prognosis and immune microenvironment in lower-grade glioma. Front Immunol 2021;12:731048.
[39] Jiang P, et al. Signatures of T cell dysfunction and exclusion predict cancer immunotherapy response. Nat Med 2018;24(10):1550–8.
[40] Fu J, et al. Large-scale public data reuse to model immunotherapy response and resistance. Genome Med 2020;12(1):21.
[41] Corsello SM, et al. Discovering the anti-cancer potential of non-oncology drugs by systematic viability profiling. Nat Cancer 2020;1(2):235–48.
[42] Meyers RM, et al. Computational correction of copy number effect improves specificity of CRISPR-Cas9 essentiality screens in cancer cells. Nat Genet 2017;49(12):1779–84.
[43] Maeser D, Gruener RF, Huang RS. oncoPredict: an R package for predicting in vivo or cancer patient drug response and biomarkers from cell line screening data. Brief Bioinform 2021;22(6).
[44] Vis DJ, et al. Multilevel models improve precision and speed of IC50 estimates. Pharmacogenomics 2016;17(7):691–700.
[45] Iorio F, et al. A landscape of pharmacogenomic interactions in cancer. Cell 2016;166(3):740–54.
[46] Rees MG, et al. Correlating chemical sensitivity and basal gene expression reveals mechanism of action. Nat Chem Biol 2016;12(2):109–16.
[47] Yang W, et al. Genomics of Drug Sensitivity in Cancer (GDSC): a resource for therapeutic biomarker discovery in cancer cells. Nucleic Acids Res 2013;41:D955–61. Database Issue.
[48] Zhang L, et al. A novel integrated system using patient-derived glioma cerebral organoids and xenografts for disease modeling and drug screening. Cancer Lett 2021;500:87–97.
[49] Verhaak RG, et al. Integrated genomic analysis identifies clinically relevant subtypes of glioblastoma characterized by abnormalities in PDGFRA, IDH1, EGFR, and NF1. Cancer Cell 2010;17(1):98–110.
[50] Ma B, et al. Reciprocal regulation of integrin β4 and KLF4 promotes gliomagenesis through maintaining cancer stem cell traits. J Exp Clin Cancer Res 2019;38(1):23.
[51] Vitanza NA, et al. Optimal therapeutic targeting by HDAC inhibition in biopsy-derived treatment-naïve diffuse midline glioma models. Neuro Oncol 2021;23(3):376–86.
[52] Qing T, et al. Somatic mutations in ZFHX4 gene are associated with poor overall survival of Chinese esophageal squamous cell carcinoma patients. Sci Rep 2017;7(1):4951.
[53] Chen A, et al. Chitinase-3-like 1 protein complexes modulate macrophage-mediated immune suppression in glioblastoma. J Clin Invest 2021;131(16).
[54] Zhao T, et al. Chitinase-3 like-protein-1 promotes glioma progression via the NF-κB signaling pathway and tumor microenvironment reprogramming. Theranostics 2022;12(16):6989–7008.
[55] Kulasekaran G, et al. An Arf/Rab cascade controls the growth and invasiveness of glioblastoma. J Cell Biol 2021;220(2).
[56] Demirdizen, E., et al., *TRIM67 drives tumorigenesis in oligodendrogliomas through Rho GTPase-dependent membrane blebbing.* Neuro Oncol, 2022.
[57] Wei C, et al. Characterization of gastric cancer stem-like molecular features, immune and pharmacogenomic landscapes. Brief Bioinform 2022;23(1).
[58] Schiffer D, et al. Glioblastoma: microenvironment and niche concept. Cancers (Basel) 2018;11(1).
[59] Caltabiano R, et al. High levels of connexin 43 mRNA in high grade astrocytomas. Study of 32 cases with in situ hybridization. Acta Histochem 2010;112(6):529–35.
[60] Silver DJ, et al. The intersection of cancer, cancer stem cells, and the immune system: therapeutic opportunities. Neuro Oncol 2016;18(2):153–9.
[61] Yan J, et al. FGL2-wired macrophages secrete CXCL7 to regulate the stem-like functionality of glioma cells. Cancer Lett 2021;506:83–94.
[62] Zhai Y, et al. Single-cell RNA-sequencing shift in the interaction pattern between glioma stem cells and immune cells during tumorigenesis. Front Immunol 2020;11:581209.
[63] Guo X, Pan Y, Gutmann DH. Genetic and genomic alterations differentially dictate low-grade glioma growth through cancer stem cell-specific chemokine recruitment of T cells and microglia. Neuro Oncol 2019;21(10):1250–62.
[64] Chen P, et al. Symbiotic macrophage-glioma cell interactions reveal synthetic lethality in PTEN-Null glioma. Cancer Cell 2019;35(6):868–84. e6.
[65] He C, et al. Single-cell transcriptomic analysis revealed a critical role of SPP1/CD44-mediated crosstalk between macrophages and cancer cells in glioma. Front Cell Dev Biol 2021;9:779319.
[66] Yang F, et al. Synergistic immunotherapy of glioblastoma by dual targeting of IL-6 and CD40. Nat Commun 2021;12(1):3424.
[67] Batlle E, Clevers H. Cancer stem cells revisited. Nat Med 2017;23(10):1124–34.
[68] Kang MK, Kang SK. Tumorigenesis of chemotherapeutic drug-resistant cancer stem-like cells in brain glioma. Stem Cells Dev 2007;16(5):837–47.
[69] Beier D, et al. Temozolomide preferentially depletes cancer stem cells in glioblastoma. Cancer Res 2008;68(14):5706–15.
[70] Alhalabi OT, et al. A novel patient stratification strategy to enhance the therapeutic efficacy of dasatinib in glioblastoma. Neuro Oncol 2022;24(1):39–51.
[71] Lassman AB, et al. Phase 2 trial of dasatinib in target-selected patients with recurrent glioblastoma (RTOG 0627). Neuro Oncol 2015;17(7):992–8.
[72] Chen R, et al. Nanomicellar TGX221 blocks xenograft tumor growth of prostate cancer in nude mice. Prostate 2015;75(6):593–602.
[73] Lee SH, et al. A constitutively activated form of the p110beta isoform of PI3-kinase induces prostatic intraepithelial neoplasia in mice. Proc Natl Acad Sci USA 2010;107(24):11002–7.
[74] Yang X, et al. TGX-221 inhibits proliferation and induces apoptosis in human glioblastoma cells. Oncol Rep 2017;38(5):2836–42.
[75] Aoki T, et al. Phase II study of ifosfamide, carboplatin, and etoposide in patients with a first recurrence of glioblastoma multiforme. J Neurosurg 2010;112(1):50–6.